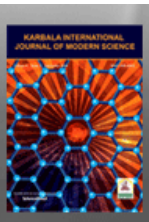

Karbala International Journal of Modern Science

Volume 8 | Issue 3 Article 23

Nuclear structure and Gamow-Teller B(GT) Transition Strengths for some Selected fp-shell Nuclei

Sarah M. Obaid
Department of Biomedical Engineering, Al-Mustaqbal University College

Fouad A. Majeed
Department of Physics, College of Education for Pure Sciences, University of Babylon,, fmajeed@uobabylon.edu.iq

Fatima Essa Mohammed
Kirkuk Education Directorate, Ministry of Education

Nuclear structure and Gamow-Teller B(GT) Transition Strengths for some Selected fp-shell Nuclei

Abstract

In the present study, the calculations of the shell model based on large-scale unrestricted fp-model space have been conducted to study the low-lying energy levels and Gamow-Teller B(GT) transition strengths for the transitions (^{42}Ca→^{42}Sc, ^{42}Sc→^{42}Ti, ^{45}Sc→^{45}Ca, ^{45}Ti→^{45}Sc,45V→^{45}Ti) lying in the fp-shell region. The calculations of the yrast levels and Gamow-Teller B(GT) transition strengths were compared with the related measured data. The low-lying energy levels were reasonably reproduced for the studied nuclei. The spin and parity of the unconfirmed energy levels for some studied nuclei have been confirmed. The calculated B(GT) transition strengths of Gamow-Teller (GT) for the selected isotopes lie in the fp-shell region agree very well with the measured data extracted from (^{3}He, t), (^{3}He, t)∗, (t,^{3}He), (t, ^{3}He+γ), and (p, n) reactions.

Keywords

Electroweak interactions, Gamow-Teller strengths, Nuclear structure, Shell model

RESEARCH PAPER

Nuclear Structure and Gamow-Teller B(GT) Transition Strengths for Some Selected fp-Shell Nuclei

Sarah M. Obaid [a], Fouad A. Majeed [b,*], Fatima E. Mohammed [c]

[a] Department of Biomedical Engineering, Al-Mustaqbal University College, Babil, Iraq
[b] Department of Physics, College of Education for Pure Sciences, University of Babylon, Babylon, Iraq
[c] Kirkuk Education Directorate, Ministry of Education, Kirkuk, Iraq

Abstract

In the present study, the calculations of the shell model based on large-scale unrestricted *fp*-model space have been conducted to study the low-lying energy levels and Gamow-Teller B(GT) transition strengths for the transitions (^{42}Ca→^{42}Sc, ^{42}Sc→^{42}Ti, ^{45}Sc→^{45}Ca, ^{45}Ti→^{45}Sc,^{45}V→^{45}Ti) lying in the *fp*-shell region. The calculations of the yrast levels and Gamow-Teller B(GT) transition strengths were compared with the related measured data. The low-lying energy levels were reasonably reproduced for the studied nuclei. The spin and parity of the unconfirmed energy levels for some studied nuclei have been confirmed. The calculated B(GT) transition strengths of Gamow-Teller (GT) for the selected isotopes lie in the *fp*-shell region agree very well with the measured data extracted from (^{3}He, t), (^{3}He, t)*, (t,^{3}He), (t, ^{3}He+γ), and (p, n) reactions.

Keywords: Electroweak interactions, Gamow-Teller strengths, Nuclear structure, Shell model

1. Introduction

Weak-interaction processes in *fp*-shell nuclei play important roles in the core-collapse stage of type II supernovae or the *rp*-process on the surface of an accreting white dwarf or neutron stars studies of electron capture and β-decay. Since the $\sigma\tau$ operator that causes the GT transitions is simple, the GT response strongly reflects the different structures of each nucleus and thus is largely different, but our knowledge of the GT transitions is very poor; therefore, there is a growing interest in determining absolute values and the distribution of GT transition intensities in stable and unstable pf-shell nuclei [1]. The response of the spin and isospin in nuclei was studied using charge-exchange processes. The change of the proton (neutron) into a proton (neutron) (isospin change $\Delta T = 1$), including or excluding spin transfer ($\Delta S = 0$ or $\Delta S = 1$) in particular, the GT transitions ($\Delta S = 1$, $\Delta T = 1$, and angular momentum transfer $\Delta L = 0$) have been extensively researched. The $\sigma\tau_{\pm}$ operator mediates these transitions, which connect the identical states between final and initial transitions as $\beta^{\pm}$decays. Understanding the late stages of star development depends on weak interaction rates [through β-decay and the capture of electron (EC)] [2–8]. J.U. Nabi et al. [9] used the deformed model of pn-QRPA to calculate the allowed transitions from charge exchange for nuclei with odd-A lying in the region of the *fp*-shell. Previous calculations (including QRPA and shell models) and observed reactions extracted from charge-exchange findings were compared with the estimated GT strength distributions. Y. Fujita et al. [10] studied the GT excitations for the nuclei with a mass number (A = 42, 46, 50, and 54) in the *fp*-shell region extracted from (^{3}He, t) reactions. In the transition ^{42}Ca →^{42}Sc reaction, the bulk of the strength of GT is distributed at the excited state with the lowest energy found at 0.6 MeV, calming that

Received 21 April 2022; revised 11 June 2022; accepted 14 June 2022.
Available online 1 August 2022

* Corresponding author at:
E-mail address: fmajeed@uobabylon.edu.iq (F.A. Majeed).

https://doi.org/10.33640/2405-609X.3253

there exists low-energy GT phonon excitation. High-energy phonon excitations in the 6–11 MeV range occur as A grows. The high-energy GT phonon excitation predominantly carries the GT strength in the ^{54}Fe→^{54}Co reaction. R. G. T. Zegers [11] studied the GT strength distribution of ^{58}Co via the ^{58}Ni (t,^{3}He) reaction. The experimental data are compared to previous data extracted from the experiments of ^{58}Ni(d,^{2}He) and ^{58}Ni(n,p) and computations of the shell model based on large-scale by employing the GXPF1 and KB3G interactions. The capture of electrons during the early stages of the supernova is a common occurrence; therefore, the distinctness between the observed data and theoretical models was investigated. Yoshida et al. [12] conducted large-scale shell-model calculations to investigate the β-decay properties of neutron-rich nuclei in 13 ≤ Z ≤ 18 and 22 ≤ N ≤ 34 by considering the first forbidden transitions. They employed full *sd* + *pf* + *sdg* valence shells, and the comparison of their results shows that the B(GT) of even–even nuclei is considerably large than neighbouring odd-A and odd–odd nuclei. S. M. Obaid and H. M. Tawfeek [13,14] studied the nuclear B(GT) of the GT transition for some *sd* and *fp*-shell nuclei. The interactions USDA and USDB have been utilized with the model space *sd*, and the FPD6, GXFP1A, and KB3G interactions were used in the model space *fp*. Their conducted study yields result that agree reasonably compared to the observed data. The transitions of the strengths GT for the transitions ^{47}Ti→^{47}V, ^{50}Cr→^{50}Mn, ^{48}Ti→^{48}V, and ^{46}Ti→^{46}V were investigated by F. A. Majeed and S. M. Obaid [15] utilize the shell model for the nuclei lies in the model space *fp* by using FPD6, GXFP1A, and KB3G interactions to predict the GT distribution for the selected nuclei, and their predicted results were contrasted with the observed data. They concluded that the observed GT distributions and their related summed B(GT) strength transitions agree reasonably well with the theoretical computations.

The present study aimed to investigate the nuclear structure of some selected isotopes in the *fp*-shell region by performing shell-model calculations using the NuShellX@MSU code [16] to calculate the excitation energy levels and B(GT) strengths. Theoretical investigation using the shell model by utilizing the full *fp*-model space will be carried out using the interactions FPD6 [17], KB3G [18], and GXFP1A [19] interactions. The predicted values for energy levels and Gamow-Teller strengths B(GT) will be analyzed and compared with the observed data, and then the conclusion of this study will be drawn.

2. Theoretical considerations

The Gamow-Teller operators have $\pi_O = +1$, and the initial and final nuclear states should therefore be $\pi_i\pi_f = +1$ for non-zero parity-transforming elements. The matrix of the elements follows the triangle $\Delta(J_f, j_i, \Delta J = 1)$. The isospin triangle state $\Delta(T_f, T_i, \Delta T = 1)$ is observed until the Gamow-Teller elements are retained. The second quantized form is of (GT_-) is then written as [20],

$$\mathcal{O}(GT_-) = \sum_{\alpha\beta} \langle \alpha | \sigma\tau_- | \beta \rangle \, a^+_{\alpha,p} \, a_{\beta,n} \,, \tag{1}$$

where $a_{\beta,n}$ annihilate neutron in β state and $a^+_{\alpha,p}$ creates the proton in α state. Thus, the form included.

J-coupling is written as [20],

$$\mathcal{O}(GT_-) = \sum_{\alpha\beta} \langle \kappa_a, p || \sigma\tau_- || \kappa_b, n \rangle \frac{\left[a^+_{\kappa_a,p} \otimes \tilde{a}_{\kappa_b,n} \right]^{\lambda}}{\sqrt{(2\lambda+1)}}, \tag{2}$$

where the operator of GT is considered as $\lambda = 1$ taken. The reduced probability between the initial i and final f states is given by [20],

$$\mathcal{O}(GT_-) = \sum_{\alpha\beta} \langle \kappa_a, p || \sigma\tau_- || \kappa_b, n \rangle OBTD(\kappa_a, \kappa_b, f, i), \tag{3}$$

where

$$OBTD(\kappa_a, \kappa_a, f, i) = \frac{\langle f \| \left[a^+_{\kappa_a,p} \otimes \tilde{a}_{\kappa_b,n} \right]^{\lambda} \| i \rangle}{\sqrt{(2\lambda+1)}}. \tag{4}$$

The equations for analogous of GT_+ are

$$\mathcal{O}(GT_+) = \sum_{\alpha\beta} \langle \alpha | \sigma\tau_+ | \beta \rangle \, a^+_{\alpha,n} a_{\beta,p}, \tag{5}$$

where $a_{\beta,p}$ annihilate proton in β state and $a^+_{\alpha,n}$ creates the neutron in α state. Thus, the form included.

J-coupling is written as [20],

$$\mathcal{O}(GT_+) = \sum_{\alpha\beta} \langle \kappa_a, n || \sigma\tau_+ || \kappa_b, p \rangle \frac{\left[a^+_{\kappa_a,n} \otimes \tilde{a}_{\kappa_b,p} \right]^{\lambda}}{\sqrt{(2\lambda+1)}}, \tag{6}$$

and the reduced transition probability is

$$\mathcal{O}(GT_+) = \sum_{\alpha\beta} \langle \kappa_a, p || \sigma\tau_+ || \kappa_a, n \rangle \, OBTD(\kappa_a, \kappa_a, f, i), \tag{7}$$

where

$$OBTD(\kappa_a,\kappa_a,f,i)=\frac{\langle f\|\left[a^{+}_{\kappa_a,n}\otimes\tilde{a}_{\kappa_b,p}\right]^{\lambda}\|i\rangle}{\sqrt{(2\lambda+1)}}. \quad (8)$$

The reduced elements of the single-particle-matrix can be written as [20].

$$\langle\kappa_a,p||\sigma\tau_{-}||\kappa_b,n\rangle=\langle\kappa_a,n||\sigma\tau_{+}||\kappa_b,p\rangle=2\langle\kappa_a||\vec{s}||\kappa_b\rangle\,, \quad (9)$$

where the elements of the matrix of $\vec{s}$ are given by

$$\langle\kappa_a||\vec{s}||\kappa_b\rangle = (-1)^{\ell_a+j_a+3/2}\sqrt{(2J_a+1)(2J_b+1)}\begin{Bmatrix}1/2 & 1/2 & 1\\ j_b & j_a & \ell_a\end{Bmatrix} \times\langle s||\vec{s}||s\rangle\delta_{\ell_a,\ell_b}\,\delta_{n_a,n_b} \quad (10)$$

with

$$<s||\vec{s}||s> \;=\sqrt{3/2}.$$

3. Results and discussion

This section contains the predicted values of the energy levels, and the strengths of B(GT) with their cumulative B(GT) values will be discussed and compared with the observed data. All the calculations are conducted using the code NushellX@MSU [16], and the B(GT) values from the theory were scaled by a factor of $(0.74)^2$.

3.1. Energy levels

3.1.1. ^{42}Ca, ^{42}Sc, and ^{42}Ti isotopes

The energy levels for the nuclei ^{42}Ca, ^{42}Sc, and ^{42}Ti lie in the *fp*-shell region have been studied by considering the core at ^{40}Ca by employing three effective interactions, GXFP1A, KB3G, and FPD6, which are designed for the *fp*-shell region. The nucleus ^{42}Ca has two valence neutrons, ^{42}Sc has a one-valence proton, one valence neutron, and ^{42}Ti has two valence protons outside the core ^{40}Ca. Fig. 1 displays the shell model calculations for ^{42}Ca, ^{42}Sc, and ^{42}Ti isotopes. All the three effective interactions precisely predict the ground state of these nuclei except for the isotope ^{42}Sc was predicted wrong as 7^+ by GXFP1A. The first 2^+ for the isotope ^{42}Ca is found experimentally at 1.525 MeV [21], and the shell model predicts the values 1.438 MeV, 1.370 MeV, and 1.781 MeV by GXFP1A, KB3G, and FPD6, respectively. The first 4^+ is found experimentally at 2.752 MeV [21], and FPD6, GXFP1A, and KB3G predict the values 2.709 MeV, 2.270 MeV, and 2.365 MeV, respectively.

There are two unconfirmed experimental data for assigned spin and parity at 3^+ and 5^+ with 4.505 MeV and 5.775 MeV values. These states are confirmed by GXFP1A with 5.519 MeV and 5.971 MeV, respectively, while KB3G predicts 4.909 MeV and 5.087 MeV, respectively. The FPD6 predicts the values at 5.147 MeV and 5.526 MeV, respectively.

The 1^+ state for ^{42}Ca is found experimentally at 4.232 MeV, and GXFP1A, KB3G, and FPD6 predict 9.165 MeV, 9.068 MeV, 9.639 MeV, respectively, which are very far from the measured value. The FPD6, GXFP1A, and KB3G could not predict the right order of the yrast energy levels for the ^{42}Sc isotope, and the first 1^+ is found experimentally at 0.616 MeV [21], and FPD6, KB3G, and GXFP1A predict the values 0.819 MeV, 0.342 MeV, and 0.306 MeV, respectively. In general, theoretical results of GXFP1A, KB3G, and FPD6 interactions are lower than measured values. The 2^+ state is found experimentally at 1.554 MeV [21] for ^{42}Ti isotope, the and GXFP1A, KB3G, and FPD6 predict the values 1.436 MeV, 1.386 MeV, and 1.746 MeV, respectively. The 4^+ state is found experimentally at 2.677 MeV [21] for the ^{42}Ti isotope, and the interactions GXFP1A, KB3G, and FPD6 predict the values at 2.269 MeV, 2.384 MeV, and 2.781 MeV, respectively. Theoretical calculations predict odd states 3^+, 5^+, and 1^+, not found in the measured data.

3.1.1. ^{45}Ca, ^{45}Sc, ^{45}Ti, and ^{45}V isotopes

Fig. 2 compares the predicted negative states and their corresponding measured data for the ^{45}Ca, ^{45}Sc, ^{45}Ti, and ^{45}V isotopes. The closed core is taken at ^{40}Ca by utilizing three interactions, namely GXFP1A, KB3G, and FPD6, designed for the *fp*-shell region. The nucleus ^{45}Ca has five valence neutrons, ^{45}Sc has a one-valence proton, four valence neutrons and ^{45}Ti have two valence protons and neutrons, consecutively, outside the core ^{40}Ca. The ground state is $7/2^-_1$ for these isotopes are precisely predicted by all the three effective interactions for all isotopes except the case of the isotopes ^{45}Ti and ^{45}V were predicted wrong as $3/2^-$ by FPD6 interaction. The first $5/2^-_1$ for the isotope ^{45}Ca is found experimentally at 0.174 MeV [21], and the shell model predicts the values 0.363 MeV, 0.195 MeV, and 0.446 MeV by KB3G and FPD6, respectively. The first $3/2^-_1$ is found measurably at 1.435 MeV [21], and GXFP1A, KB3G, and FPD6 predict 1.118 MeV, 1.110 MeV, and 1.522 MeV, respectively. There are two unconfirmed experimental levels for ^{45}Ca assigned on $11/2^-_1$ and $15/2^-_1$ with values of 1.554 MeV and 2.878 MeV. These states have been confirmed by GXFP1A at 1.393 MeV and 2.578 MeV,

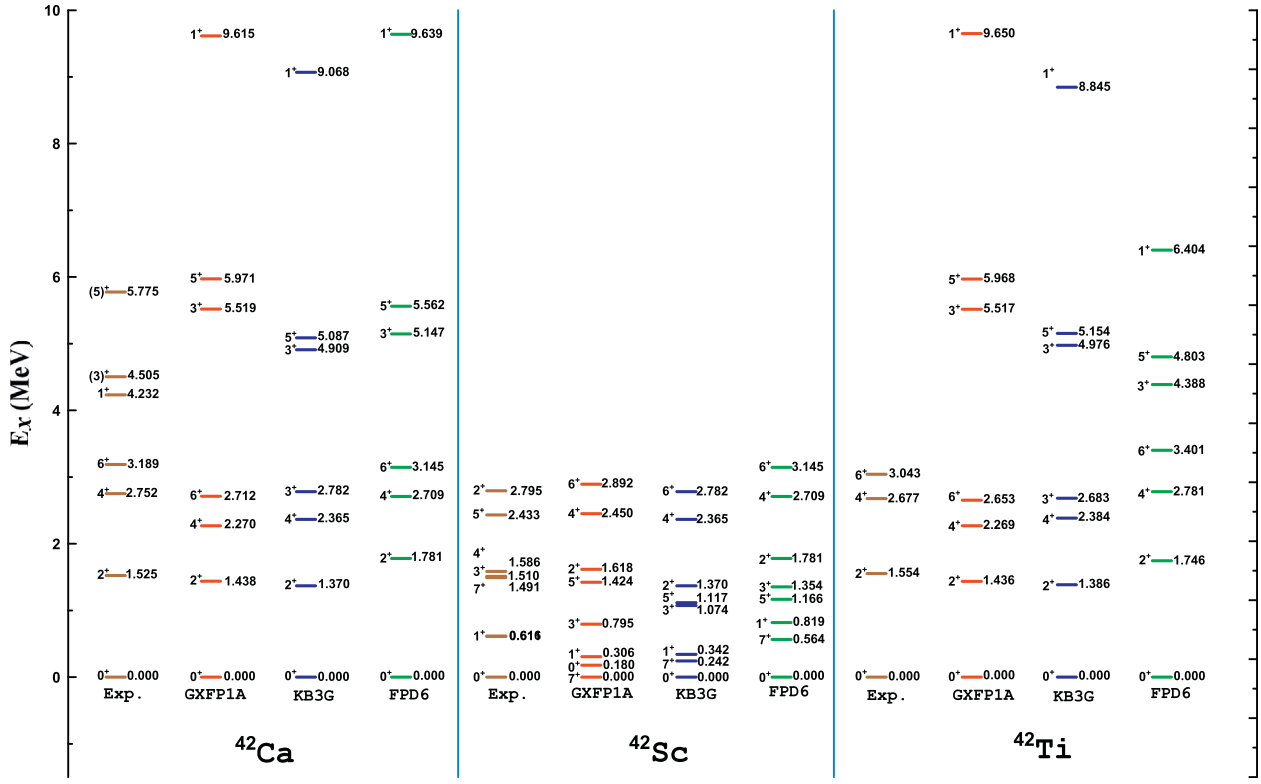

Fig. 1. Displays a comparison of predicted yrast levels for ^{42}Ca, ^{42}Sc, and ^{42}Ti isotopes using FPD6, GXFP1A, and KB3G and interactions with the observed data.

respectively, while KB3G predicts the values of 1.371 MeV and 2.600 MeV, respectively FPD6 predicts the values at 1.661 MeV and 2.973 MeV. The first $3/2^-_1$ for ^{45}Sc is found experimentally at 0.337 MeV [21] and the GXFP1A, KB3G and FPD6 interactions predict the values 1.033 MeV, 0.777 MeV and 0.666 MeV, respectively. The first $5/2^-_1$ is found experimentally at 0.720 MeV [21], and the

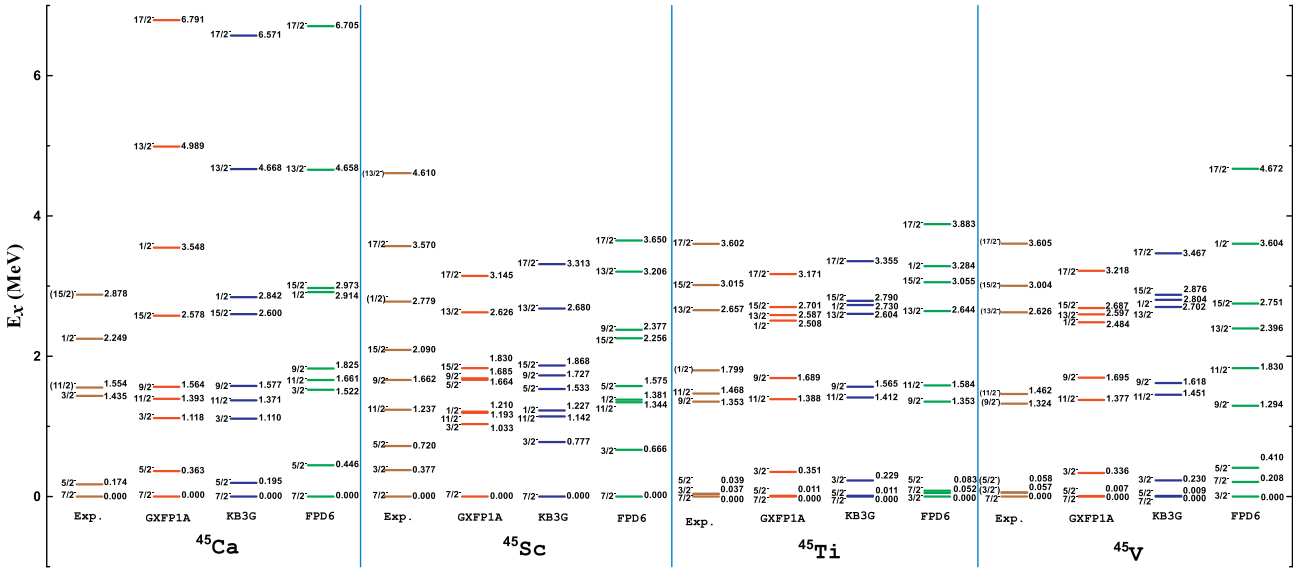

Fig. 2. Displays a comparison of predicted yrast levels for ^{45}Ca, ^{45}Sc, ^{45}Ti, and ^{45}V isotopes using FPD6, GXFP1A, and KB3G and interactions with the observed data.

interactions GXFP1A, KB3G, and FPD6 predict the values as 1.664 MeV, 1.533 MeV, and 1.575 MeV, respectively. The three interactions did not predict the right order of the yrast levels for the ^{45}Sc isotope. There is one unconfirmed level in the measured data that has assigned spin and parity $1/2_1^-$ with a value of 2.779 MeV and the FPD6, GXFP1A, and KB3G and interactions estimate the values 1.381 MeV, 1.210 MeV, and 1.227 MeV with a difference of an order of magnitude~0.1 MeV. Experimentally the first excited level for ^{45}Ti is $3/2^-$ is observed at 0.037 MeV [21], while the interactions FPD6, KB3G, and GXFP1A estimate the values 0.351 MeV, 0.229 MeV, and 0.000 MeV, respectively. The only unconfirmed level measured for the ground state band is $1/2_1^-$ with the value of 1.799 MeV, and GXFP1A, KB3G, and FPD6 predict the values of 2.508 MeV, 2.730 MeV, and 3.284 MeV, respectively. The only confirmed level is the ground state for the isotope ^{45}V. The rest levels in the ground states are unconfirmed experimentally; our theoretical results with the three interactions confirm most of these levels using GXFP1A, KB3G, and FPD6 interactions, as shown in Fig. 2.

3.2. The B(GT) results

3.2.1. $^{42}Ca \rightarrow {}^{42}Sc$

The calculated B(GT) values by shell model utilizing the full model space *fp* and the observed data for the transition ^{42}Ca→^{42}Sc are depicted in Fig. 3. The B(GT) values are predicted from the lowest level of ^{42}Sc (0^+) to ^{42}Ca (1^+) levels using the FPD6, KB3G, and GXFP1A interactions. The observed charge-exchange reaction via ^{42}Ca(^{3}He,t)^{42}Sc [22]. The shell model predictions of the strengths of B(GT) have been damped by $(0.74)^2$ factor to suit the observed data, following a good deal of prior research conducted by various authors. Fig. 4 displays the cumulative values of B(GT) versus the excitation energy of ^{42}Sc. Theoretical summed value of B(GT) with three interactions is lower than observed data for the excitation energy range, approximately from 3 MeV to 9.5 MeV; this is due to the contribution coming from the first dominated high value of B(GT) located at 0.612 MeV with B(GT) value 2.173 [12]. Theoretical summed B(GT) overshoots the observed data in the excitation range of approximately 9.5 MeV−14.5 MeV due to the peaks in theory distributed from ~8.7 MeV to ~9.8 MeV.

3.2.2. $^{42}Ti \rightarrow {}^{42}Sc$

Fig. 5 depicts the predicted strengths for the GT for ^{42}Ti (0^+) transition from the lowest state to the excited states (1^+) in ^{42}Sc. The observed data are taken from the reactions in ^{42}Sc, available from ^{42}Ti(β^+) measured [22], and the predicted values using the interactions FPD6, GXFP1A, and KB3G. They are only two measured values one very weak located at excitation energy $E_x(^{42}Sc) = 0.611$ MeV, and the second dominated strong peak located at excitation energy $E_x(^{42}Sc) = 1.888$ MeV with observed B(GT) values at 0.059 and 2.313, respectively. The FPD6, GXFP1A, and KB3G predicted the strongest peak at 0.0 MeV with B(GT) values 2.648, 2.343, and 2.509, consecutively. The dominant observed peaks were found in the transition ^{42}Ti (0^+) →^{42}Sc(1^+) in the ^{42}Ti(^{3}*He*, *t*) reaction, which does not agree with the theoretically predicted value that is calculated from the transition

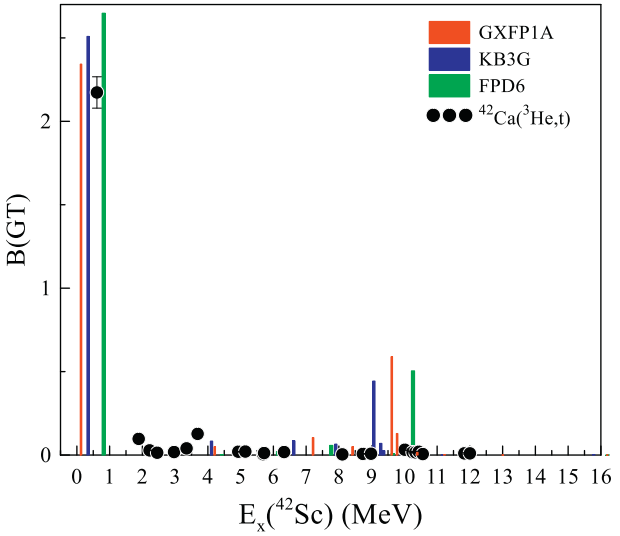

Fig. 3. Displays theoretical B(GT) values compared to the measured data [22] for $^{42}Ca \rightarrow {}^{42}Sc$.

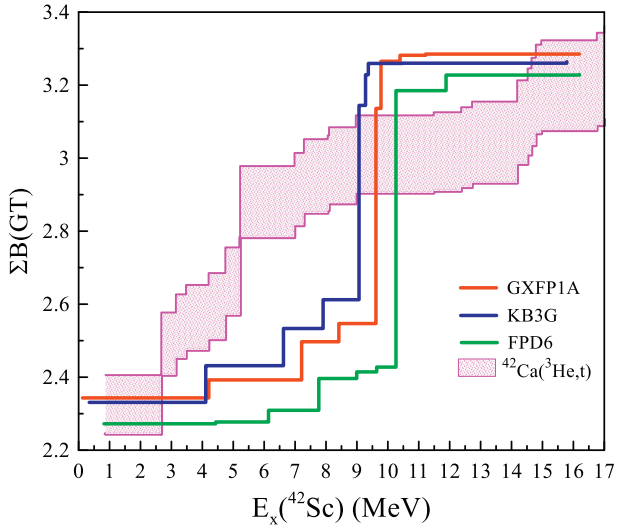

Fig. 4. Displays the $\sum \mathbf{B(GT)}$ compared to the observed data for $^{42}Ca \rightarrow {}^{42}Sc$.

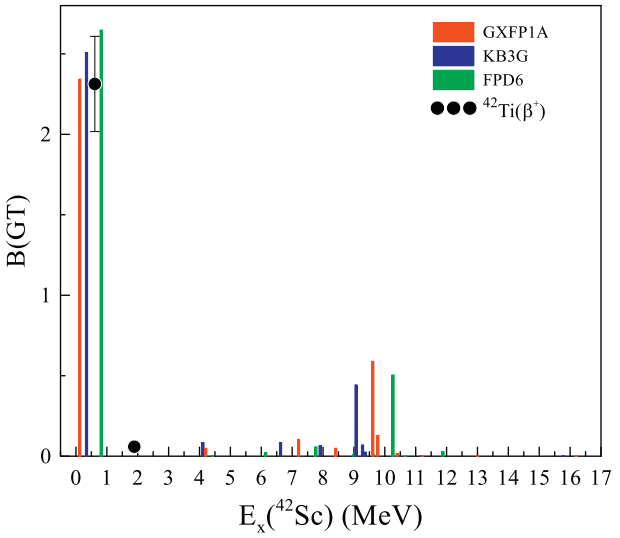

Fig. 5. Displays theoretical B(GT) values compared to the measured data [23] for $^{42}Ti \rightarrow {}^{42}Sc$.

^{42}Ti(0^+)→^{42}Sc(1^+) for the interactions FPD6, GXFP1A, and KB3G, while the predicted B(GT) distribution values from the rest of the transitions are weak. The employed interactions correctly predicted the spin and parity for the ground state of both ^{42}Ti and ^{42}Sc. Fig. 6 compares the summed B(GT) values predicted by GXFP1A, KB3G, and FPD6 and the observed data. Since we have just two measured values, this comparison is unreliable; once we have more measured data in the future, we can compare them with our results.

3.2.3. $^{45}Sc \rightarrow {}^{45}Ca$

Fig. 7 depicts the strengths of B(GT) for ^{45}Sc 7/2$^-$ lowest state to the excited states in ^{45}Ca with J^π = (5/2$^-$, 7/2$^-$, 9/2 $^-$). The observed data are available from the reactions ^{45}Sc(p,n)^{45}Ca [24] and ^{45}Sc(t,^{3}He+γ) [25]. The predicted shell model in full f p model space has been performed using FPD6, GXFP1A, and KB3G. The measured data are from ^{45}Sc(p,n)^{45}Ca [23] and the B(GT) values are weak, and the peak is located at excitation energy E$_x$(^{45}Ca) = 7.123 MeV with a value of 0.183 MeV. The interactions FPD6, GXFP1A, and KB3G predicted the strongest peak at E$_x$(^{45}Ca) = 5.278 MeV, 6.098 MeV, and 6.005 MeV with estimated B(GT) at 0.370, 0.307, and 0.509, consecutively. The parity and spin of the ground state level for both ^{45}Sc and ^{45}Ca were predicted correctly by all the three interactions. The B(GT) values calculations by GXFP1A and KB3G interactions are very small at

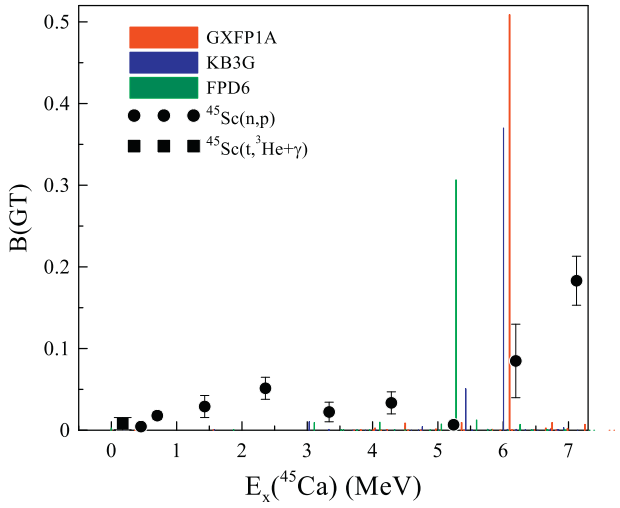

Fig. 7. Displays theoretical B(GT) values compared to the measured data [24,25] for $^{45}Sc \rightarrow {}^{45}Ca$.

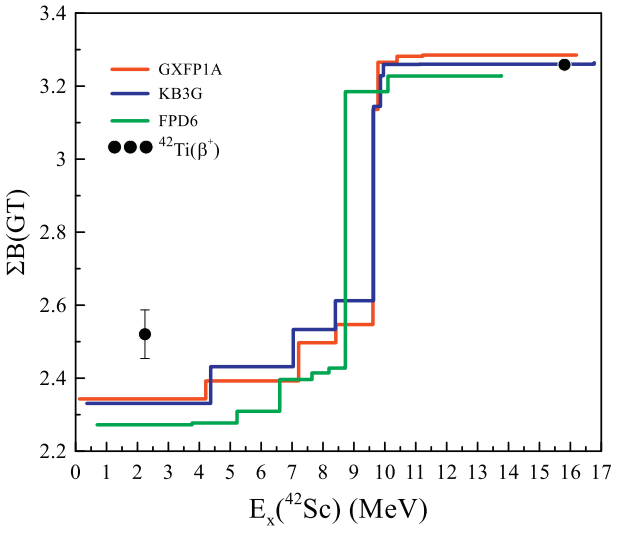

Fig. 6. Displays the $\sum \mathbf{B(GT)}$ compared to the observed data for $^{42}Ti \rightarrow {}^{42}Sc$.

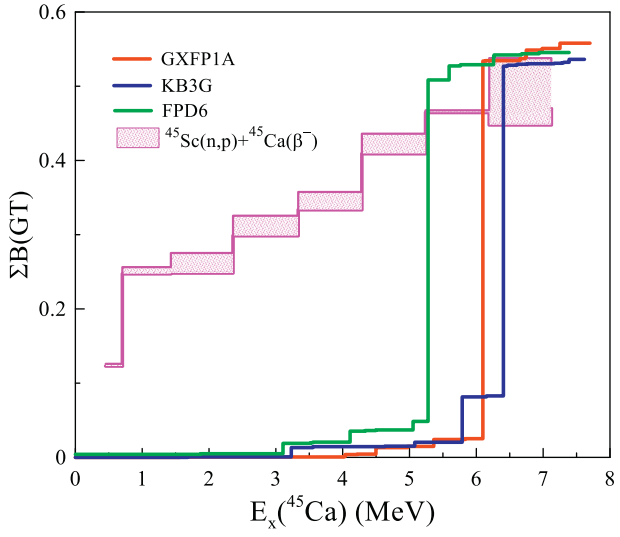

Fig. 8. Displays the $\sum \mathbf{B(GT)}$ compared to the observed data for $^{45}Sc \rightarrow {}^{45}Ca$.

zero in the excitation energy range E_x (^{45}Ca) = 0~3 MeV. Fig. 8 depicts the comparison of the summed B(GT) predicted by FPD6, GXFP1A, and KB3G along with the related observed data; we can see that there is a big discrepancy between theory and observed data for all three effective interactions in the excitation energy range E_x(^{45}Ca) ≈0 → 5 MeV and this is due to the fact the prediction of the B(GT) values is zero or very small as explained before.

3.2.4. $^{45}Ti \rightarrow {}^{45}Sc$

Fig. 9 illustrates the predicted B(GT) for ^{45}Ti ($7/2^-$) starting from the lowest state to the excited states J^π = ($5/2^-$, $7/2^-$, $9/2^-$) in ^{45}Sc. The observed data for ^{45}Ti is found from the reaction ^{45}Ti(^3He, t)^{45}Sc [26]. The predicted B(GT) values from the shell-model by employing FPD6, KB3G, and GXFP1A shows that there are only four observed values with dominant peak located at E_x(^{45}Sc) = 0.02 MeV with predicted B(GT) at 0.0973 and the rest three peaks located at Ex(45Sc) = 0.74 MeV, E_x(^{45}Sc) = 1.4 MeV, and E_x(^{45}Sc) = 1.64 MeV with predicted B(GT) at 0.01, 0.002, and 0.005, consecutively. The FPD6, KB3G, and GXFP1A predicted the strongest peak at E^x(^{45}Ca) = 0.0 MeV with B(GT) values 0.131, 0.104, and 0.089, respectively. The other predicted values are almost the same value by the three interactions, which agree with the experiment's last two values of B(GT). The spin and parity of the ground state for both ^{45}Ti and ^{45}Sc were predicted correctly by all the three interactions except for ^{45}Sc, and the FPD6 interaction predicted wrong the ground state. Fig. 10 shows the summed B(GT) compared to the predicted shell model values using the employed

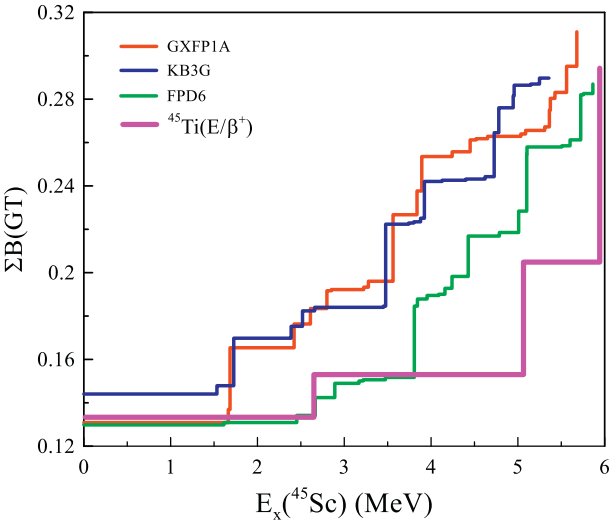

Fig. 10. Displays the $\sum \mathbf{B(GT)}$ compared to the observed data for $^{45}Ti \rightarrow {}^{45}Sc$.

interactions with the observed values. The best agreement with observed data is the calculation from the FPD6 interaction. The present calculations agree with the results obtained by Kumar et al. [27].

3.2.5. $^{45}V \rightarrow {}^{45}Ti$

The predicted B(GT) strengths for ^{45}V→^{45}Ti transition. There is no measured data available for this transition, and we have presented just theoretical calculations using the three interactions, FPD6, GXFP1A, and KB3G, as shown in Fig. 11. As we can see from theoretical results, three dominant peaks are predicted by the three effective interactions. Fig. 12 displays the summed B(GT), where all the interactions have the same behaviour of

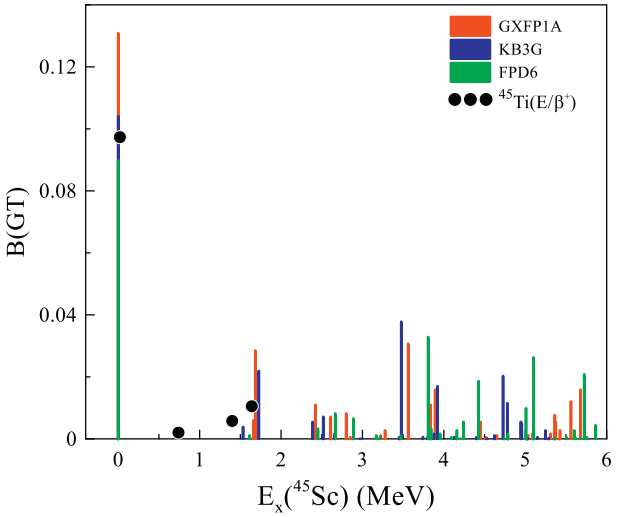

Fig. 9. Displays theoretical B(GT) values compared to the measured data [26] for $^{45}Ti \rightarrow {}^{45}Sc$.

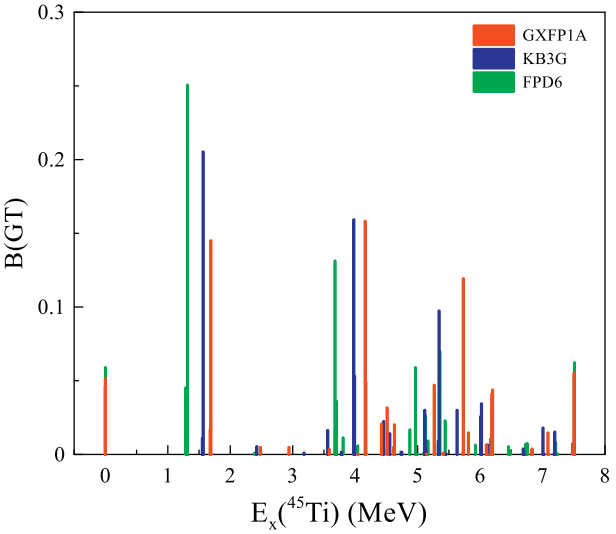

Fig. 11. Displays theoretically predicted B(GT) values compared to the measured data [27] for $^{45}V \rightarrow {}^{45}Ti$.

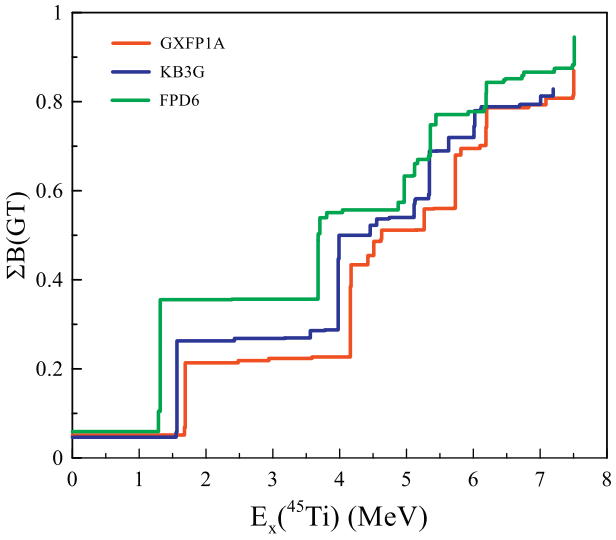

Fig. 12. Displays the $\sum \mathbf{B}(\mathbf{GT})$ *compared to the observed data for* $^{45}V \rightarrow {}^{45}Ti$.

calculations. These theoretical results might be compared once available data for this transition.

4. Conclusion

The study detailed a theoretical investigation of the nuclear structure for some selected isotopes in the *fp*-shell region. The shell model framework has been employed to study the ground state energy levels and the strength of B(GT). The ground state spin and parity for all the studied isotopes in the *fp*-shell region were precisely predicted by utilizing the shell model computations with FPD6, GXFP1A, and KB3G residual interactions for *fp*-shell, except for ^{45}Ti and ^{45}V isotopes where the ground state is $7/2^-$ and FPD6 predict wrong the ground state as $3/2^-$. The calculation of B(GT) strengths for the studied transitions for the isotopes lie in the *fp*-shell region using FPD6, GXFP1A, and KB3G shows a fair match with the available observed data. The present study added extra information for researchers interested in the *fp*-shell region. A fair qualitative compromise was reached for individual transitions of B(GT).

Conflict of interest

The authors have no conflicts of interest to declare.

Acknowledgements

The author S.M. Obaid gratefully acknowledged the financial support provided by Al-Mustaqbal University College.

References

[1] K. Langanke, G. Martõnez-Pinedo, Nuclear weak-interaction processes in stars, Rev Mod Phys. 75 (3) (2003) 819, https://doi.org/10.1103/RevModPhys.75.819.
[2] G.M. Fuller, W.A. Fowler, M.J. Newman, Stellar weak-interaction rates for sd-shell nuclei. I- Nuclear matrix element systematics applied to 26Al and selected nuclei of importance to the supernova problem, Astrophys J Suppl. 42 (1980) 447, https://doi.org/10.1086/190657.
[3] G.M. Fuller, W.A. Fowler, M.J. Newman, Stellar weak interaction rates for intermediate-mass nuclei. II-A=21 to A=60, Astrophys J. 252 (2) (1982) 715–740, https://doi.org/10.1086/159597.
[4] G.M. Fuller, W.A. Fowler, M.J. Newman, Stellar weak interaction rates for intermediate-mass nuclei.III. Rate tables for the nucleons with A = 21 to A = 60, Astrophys J Suppl. 48 (3) (1982) 279–319, https://doi.org/10.1086/190779.
[5] G.M. Fuller, W.A. Fowler, M.J. Newman, Stellar weak interaction rates for intermediate-mass nuclei. IV-Interpolation procedures for rapidly varying lepton capture rates using effective log (ft)-values, Astrophys J. 293 (1985) 1–16, https://doi.org/10.1086/163208.
[6] A. Heger, K. Langanke, G. Martínez-Pinedo, S.E. Woosley, Presupernova collapse models with improved weak-interaction rates, Phys Rev Lett. 86 (9) (2001) 1678, https://doi.org/10.1103/PhysRevLett.86.1678.
[7] S. E. Woosley Heger, G. Martí, K. Langanke, Presupernova evolution with improved rates for weak interactions, Astrophys J. 560 (1) (2001) 307, https://doi.org/10.1086/324092.
[8] K. Langanke, G. Martí, J.M. Sampaio, D.J. Dean, W.R. Hix, O. E.B. Messer, A. Mezza- cappa, M. Liebendörfer, H. T. Janka, M. Rampp, Electron capture rates on nuclei and implications for stellar core collapse, Phys Rev Lett. 90 (24) (2003), 241102, https://doi.org/10.48550/arXiv. astro-ph/0302459.
[9] J.-U. Nabi, M. Majid, M. Riaz, Allowed Gamow-teller strength distributions and stellar electron capture rates on odd-A nuclei, Int J Mod Phys: Conf Ser. 49 (2019), 1960009, https://doi.org/10.1142/S2010194519600097.
[10] Y. Fujita, H. Fujita, T. Adachi, C.L. Bai, A. Algora, G.P.A. Berg, P. von Brentano, G. Coló, M. Csatlos, J.M. Deaven, E. Estevez-Aguado, C. Fransen, D. De Frenne, K. Fujita, E. Ganioglu, C.J. Guess, J. Gulyas, K. Hatanaka, K. Hirota, M. Honma, D. Ishikawa, E. Jacobs, A. Krasznahorkay, H. Matsubara, K. Matsuyanagi, R. Meharchand, F. Molina, K. Muto, K. Nakanishi, A. Negret, H. Okamura, H.J. Ong, T. Otsuka, N. Pietralla, G. Perdikakis, L. Popescu, B. Rubio, H. Sagawa, P. Sarriguren, C. Scholl, Y. Shimbara, Y. Shimizu, G. Susoy, T. Suzuki, Y. Tameshige, A. Tamii, J.H. Thies, M. Uchida, T. Wakasa, M. Yosoi, R.G.T. Zegers, O. Zell, J. Zenihiro, Observation of low- and high-energy gamow-teller phonon excitations in nuclei, Phys Rev Lett. 112 (11) (2014), 112502, https://doi.org/10.1103/PhysRevLett.112.112502.
[11] R.G.T. Zegers, Measurement of weak rates for stellar evolution via the (t,3He) reaction, Nucl Phys. 787 (1–4) (2007) 329–336, https://doi.org/10.1016/j.nuclphysa.2006.12.052.
[12] S. Yoshida, Y. Utsuno, N. Shimizu, T. Otsuka, Systematic shell-model study of β-decay properties and Gamow-Teller strength distributions in A ≈ 40 neutron-rich nuclei, Phys Rev C. 97 (2018), 054321, https://doi.org/10.1103/PhysRevC.97.054321.
[13] S.M. Obaid, H.M. Tawfeek, Gamow-Teller strengths of some sd-shell nuclei in the shell model framework, Rev Mexic Fisica. 66 (3) (2020) 330–335, https://doi.org/10.31349/revmexfis.66.
[14] S.M. Obaid, H.M. Tawfeek, Investigation of strengths distributions of Gamow-Teller in *sd* and *fp* shell nuclei, IOP Conf Ser Mater Sci Eng. 871 (1) (2020), 012086, https://doi.org/10.1088/1757-899X/871/1/012086.

[15] F.A. Majeed, S.M. Obaid, Calculations of gamow–teller transition strengths in fp-shell nuclei using shell model, Can J Phys. 99 (1) (2021) 33–37, https://doi.org/10.1139/cjp-2019-0693.
[16] B.A. Brown, W.D.M. Rae, The shell-model code NuShellX@ MSU, Nucl Data Sheets. 120 (1) (2014) 115–118, https://doi.org/10.1016/j.nds.2014.07.022.
[17] W.A. Richter, M.G. Van Der Merwe, R.E. Julies, B.A. Brown, New effective interactions for the 0f1p shell, Nucl Phys A. 523 (2) (1991) 325, https://doi.org/10.1016/0375-9474(91)90007-S.
[18] A. Poves, J. Snchez-Solano, E. Caurier, F. Nowacki, Shell model study of the isobaric chains A=50, A=51, and A=52, Nucl Phys A. 694 (1–2) (2001) 157, https://doi.org/10.1016/S0375-9474(01)00967-8.
[19] M. Honma, T. Otsuka, B.A. Brown, T. Mizusaki, New effective interaction for pf -shell nuclei and its implications for the stability of the N=Z= 28 closed core, Eur Phys J A. 25 (S1) (2005) 499, https://doi.org/10.1103/PhysRevC.69.034335.
[20] A. Brown, B.H. Wildenthal, Corrections to the free-nucleon values of the single-particle matrix elements of the m1 and Gamow-teller operators, from a comparison of shell-model predictions with sd-shell data, Phys Rev C. 28 (6) (1983) 2397–2413, https://doi.org/10.1103/PhysRevC.28.2397.
[21] Evaluated nuclear structure data file (database 15-12-2021), Accessed online 15-1-2022, https://www.nndc.bnl.gov/ensdf/.
[22] T. Adachi, Y. Fujita, P. Von Brentano, N. Bothac, H. Fujita, H. Hashimoto, K. Hatanaka, M. Matsubara, K. Nakanishi, R. Levelingz, T. Ohta, Y. Sakemi, Y. Shimbara, Y. Shimizu, C. Scholl, Y. Tameshige, A. Tamii, R. Zegers, Gamow-Teller strengths in A = 42 isobars deduced in the combined analysis of Tz = ±1 to 0 mirror transitions, in: Os- aka university laboratory of nuclear studies, Osaka University Laboratory of Nuclear Studies, Osaka/Japan, 2006.
[23] F. Molina, B. Rubio, Y. Fujita, W. Gelletly, J. Agramunt, A. Algora, J. Benlliure, P. Boutachkov, L. Caceres, R. B. Cakirli, E. Casarejos, C. Domingo-Pardo, P. Doornenbal, A. Gadea, E. Ganioğğlu, M. Gascõn, H. Geissel, J. Gerl, M. Górska, J. Grebosz, R. Hoischen, R. Kumar, N. Kurz, I. Kojouharov, L. A. Susam, H. Matsubara, A. I. Morales, A. Oktem, Y. Oktem, D. Pauwels, D. Perez-Loureiro, S. Pietri, Zs. Podolyák, W. Prokopowicz, D. Rudolph, H. Schaffner, S. J. Steer, J. L. Tain, A. Tamii, S. Tashenov, J.J. Valiente-Dobón, S. Verma, H-J. Wollersheim, $T_z = -1 \rightarrow 0$ β-decays of ^{54}Ni,^{50} Fe,^{46} Cr, and ^{42}Ti and comparison with mirror (^{3}He), measurements, Phys. Rev. C. vol. 91 (1) (2015), 014301, https://doi.org/10.1103/PhysRevC.91. 014301.
[24] W. Alford, A. Celler, B. Brown, R. Abegg, K. Ferguson, R. Helmer, K. Jackson, S. Long, K. Raywood, S. Yen, Measurement of Gamow-Teller and spin dipole strength in the 45sc (n, p) 45Ca reaction at 198 MeV, Nucl Phys. 531 (1) (1991) 97, https://doi.org/10.1016/0375-9474(91)90571-M, 11.
[25] S. Noji, R.G.T. Zegers, S.M. Austin, T. Baugher, D. Bazin, B. A. Brown, C. M. Campbell, A. L. Cole, H. J. Doster, A. Gade, C. J. Guess, S. Gupta, G. W. Hitt, C. Langer, S. Lipschutz, E. Lunderberg, R. Marchand, Z. Meisel, G. Perdikis, J. Pereira, F. Recchia, H. Schatz, M. Scott, S. R. Stroberg, C. Sullivan, L. Valdez, C. Walz, D. Weisshaar, S. J. Williams, K. Wimmer, Gamow-teller transitions to ^{45}Ca via the ^{45}Sc (t,3 He + γ) reaction at 115 MeV/u and its application to stellar electron-capture rates, Phys Rev C. 92 (2015), 024312, https://doi.org/10.1103/PhysRevC.92.024312.
[26] T.W. Burrows, Nuclear data sheets update for A = 45, Nucl Data Sheets. 65 (1) (1992) 1–63, https://doi.org/10.1016/0090-3752(92)80005-5.
[27] T. Kumar, P.C. Srivastava, A. Kumar, Gamow-Teller transition strengths for selected *fp* shell nuclei, Acta Phys Pol B. 51 (4) (2020) 961–972, https://doi.org/10.1016/j.nds.2007.12.002.